PHYSICAL REVIEW B **96**, 184503 (2017)

Correlation between non-Fermi-liquid behavior and superconductivity in (Ca, La)(Fe,Co)As_2 iron arsenides: A high-pressure study

W. Zhou,[1,2] F. Ke,[3] Xiaofeng Xu,[1,*] R. Sankar,[4,5] X. Xing,[2] C. Q. Xu,[1] X. F. Jiang,[1] B. Qian,[1,†] N. Zhou,[2] Y. Zhang,[2] M. Xu,[2] B. Li,[6] B. Chen,[3] and Z. X. Shi[2,‡]

[1]*Advanced Functional Materials Laboratory and Department of Physics, Changshu Institute of Technology, Changshu 215500, China*
[2]*School of Physics and Key Laboratory of MEMS of the Ministry of Education, Southeast University, Nanjing 211189, China*
[3]*Center for High Pressure Science and Technology Advanced Research, Shanghai 201203, China*
[4]*Institute of Physics, Academia Sinica, Nankang, Taipei 11529, Taiwan, Republic of China*
[5]*Center for Condensed Matter Sciences, National Taiwan University, Taipei 10617, Taiwan, Republic of China*
[6]*College of Science, Nanjing University of Posts and Telecommunications, Nanjing 210023, China*

(Received 4 July 2017; revised manuscript received 21 October 2017; published 3 November 2017)

Non-Fermi-liquid (NFL) phenomena associated with correlation effects have been widely observed in the phase diagrams of unconventional superconducting families. Exploration of the correlation between the normal state NFL, regardless of its microscopic origins, and the superconductivity has been argued as a key to unveiling the mystery of the high-T_c pairing mechanism. Here we systematically investigate the pressure-dependent in-plane resistivity (ρ) and Hall coefficient (R_H) of a high-quality 112-type Fe-based superconductor $Ca_{1-x}La_xFe_{1-y}Co_yAs_2$ ($x = 0.2$, $y = 0.02$). With increasing pressure, the normal-state resistivity of the studied sample exhibits a pronounced crossover from non-Fermi-liquid to Fermi-liquid behaviors. Accompanied with this crossover, T_c is gradually suppressed. In parallel, the extremum in the Hall coefficient $R_H(T)$ curve, possibly due to anisotropic scattering induced by spin fluctuations, is also gradually suppressed. The symbiosis of NFL and superconductivity implies that these two phenomena are intimately related. Further study on the pressure-dependent upper critical field reveals that the two-band effects are also gradually weakened with increasing pressure and reduced to the one-band Werthamer-Helfand-Hohenberg limit in the low-T_c regime. Overall, our paper supports the picture that NFL, multigap, and extreme $R_H(T)$ are all of the same magnetic origin, i.e., the spin fluctuations in the 112 iron arsenide superconductors.

DOI: 10.1103/PhysRevB.96.184503

I. INTRODUCTION

Exploring the unusual normal state of high-temperature (high-T_c) superconductors is arguably one of the most important tools to pry into the high-T_c superconductivity mechanism [1–5]. In the two largest high-T_c families, namely, cuprates and iron-based superconductors, a significant deviation from the quadratic T dependence of resistivity that is expected from Landau's Fermi-liquid (FL) theory has been found just above the superconducting dome, revealing the close tie between non-Fermi-liquid (NFL) excitations and the high-T_c superconductivity [1,4]. Besides the NFL phenomenon, iron-based superconductors also display other extraordinary transport behaviors, such as a strong T-dependent Hall coefficient R_H [6,7], sign changes in $R_H(T)$ curves [8,9], and the violation of Kohler's scaling [10,11]. As a consequence of the close proximity between the antiferromagnetic (AFM) order and superconductivity in the phase diagram, a very plausible origin for these anomalous transport properties is the spin fluctuation (SF), which may also serve as the pairing glue for the high-T_c superconductivity.

In iron pnictides, the normal-state resistivity has often been extensively described by the power-law dependence, $\rho = \rho_0 + AT^\alpha$, in which $\alpha = 2$ corresponds to FL ground states [12–15]. Deviations from FL ($1 < \alpha < 2$) have been observed in both the under- and overdoped regions, revealing a remarkable V-shaped dependence of the exponent α on doping [14,15]. The observation of $\alpha = 1$ at the optimal doping seemingly supports the magnetic quantum critical point (QCP) scenario. However, there is also a lot of evidence showing that NFL behavior could be a new state of matter in its own right rather than a consequence of the QCP. For example, in $Ce_{1-x}Yb_xCoIn_5$, NFL regimes and superconductivity persist in samples with and without QCP [16]. In Co-doped LiFeAs, which is regarded as a simple system because neither magnetic nor structural transitions have been detected in the phase diagram, the NFL region is found to shift to the boundary of the superconducting phase [12]. Currently, the relationship between the normal-state NFL, QCP, and superconductivity, especially in connection with SFs, is still a matter of considerable controversy.

Recently, novel 112-type superconductors $Ca_{1-x}RE_xFeAs_2$ (RE = rare-earth element) were discovered and provided a new platform to study the relationship between NFL and unconventional superconductivity [17,18]. For the 112 system, it is theoretically predicted that the parent phase $CaFeAs_2$ is a spin-density-wave type of striped antiferromagnet driven by Fermi-surface nesting [19], similar to many other Fe-based superconductors. However, no experimental synthesis of pure $CaFeAs_2$ has yet been achieved. As shown in the summarized phase diagram in Fig. 1, doping $CaFeAs_2$ with La can stabilize a high-T_c superconductivity over 35 K [17,20]. For samples with La doping level $0.15 \leqslant x \leqslant 0.24$, AFM-like transitions were claimed from ^{75}As-nuclear magnetic resonance (NMR), and the Néel temperature T_N was intriguingly found to increase

*xiaofeng.xu@cslg.edu.cn
†njqb@cslg.edu.cn
‡zxshi@seu.edu.cn

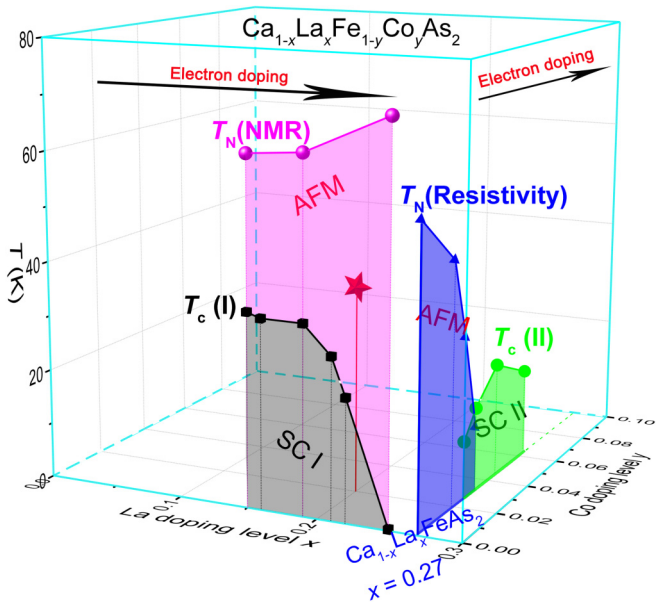

FIG. 1. The electronic phase diagram for 112-type Fe-based superconductor $Ca_{1-x}La_xFe_{1-y}Co_yAs_2$ based on previous experimental results [20,22]. For $Ca_{1-x}La_xFeAs_2$, the AFM transition temperature T_N grows with increasing electron doping from La substitution on the Ca site, while, for $Ca_{1-x}La_xFe_{1-y}Co_yAs_2$ ($x = 0.27$), T_N is gradually suppressed with electron doping from Co substitution on the Fe site. The sample labeled by the red star is the 112 superconductor $Ca_{1-x}La_xFe_{1-y}Co_yAs_2$ ($x = 0.2$, $y = 0.02$, $T_c \sim 37.5$ K at ambient pressure) used for the high-pressure study in this paper.

with x [20], in stark contrast to many existing Fe-based superconductors. Later, a lower T_N (∼58 K) was observed from the resistivity anomaly at $x = 0.27$ by another group [21]. More intriguingly, if one further introduces electron doping through Cobalt co-doping for Fe or application of high pressure on sample $Ca_{1-x}La_xFeAs_2$ ($x = 0.27$), AFM transition is found to be gradually suppressed and a seemingly second superconducting phase with a maximum T_c around 25 K is resolved [22,23]. It appears that sample $Ca_{1-x}La_xFeAs_2$ ($x = 0.27$) plays the role of the *parent phase* for the second superconducting regime. Such an interesting phase diagram with multiple electronic orders is rarely seen in other high-T_c superconducting systems, making the 112-type superconductors a unique platform to study the interplay between the normal-state transport and superconductivity.

In this paper, we have selected the high-quality single crystal $Ca_{1-x}La_xFe_{1-y}Co_yAs_2$ ($x = 0.2$, $y = 0.02$, $T_c \sim 37.5$ K), the normal state of which exhibits pronounced departure from the Fermi-liquid picture [24], as a candidate to perform the high-pressure study. Compared with chemical substitutions, high pressure has proven to be a clean way to tune the electronic properties of a material as no additional impurity effects are introduced. Unfortunately, a high-pressure study of the correlation between the normal-state transport and high-T_c superconductivity on 112 iron pnictides is still lacking. In this paper, we aim to achieve a fine tuning of the normal-state transport and superconductivity via pressure, and thus investigate the correlation between NFL and superconductivity in this 112 iron pnictide. As we found, at low pressures, the normal state of the sample exhibits obvious deviation from the conventional FL behaviors. Especially, T-linear resistivity without signature of possible QCP is observed at the optimal pressure ($P = 3.9$ GPa) where T_c reaches the highest value. Above $P = 17$ GPa where superconductivity is totally suppressed, the normal-state FL behaviors emerge. No trace of a second superconducting phase can be identified up to 40 GPa. We discussed our results in terms of the role of SFs on both the normal-state transport and superconductivity in this 112 Fe-based system.

II. EXPERIMENT

Single crystals of $Ca_{1-x}La_xFe_{1-y}Co_yAs_2$ ($x = 0.2$, $y = 0.02$) were grown by FeAs self-flux method as described elsewhere [25,26]. Good single crystallinity of the as-grown samples was confirmed by a single-crystal x-ray-diffraction measurement [26]. The electrical pressure experiments were performed using a screw-type diamond anvil cell. A pair of anvil culets of 500 μm was used at the top and the bottom of the pressure chamber, the diameter of which is about 100 μm. Four electrodes were made on the surface of the freshly cleaved crystal of size ∼70 μm in length or width and 15 μm in thickness [see the pressure setup in the upper-left inset in Fig. 2(a)]. Afterward, the sample together with ruby spheres for pressure calibration was loaded into the center of the pressure chamber. The transmitting medium (Daphne 7373) was injected to ensure a quasi-isotropic pressure environment. For discussion of the pressure uniformity issue, see Ref. [27]. Pressure was calibrated by the measurements of the peak shift in the Raman spectroscopy (laser wavelength ∼514.5 nm) of the ruby spheres or the diamond anvil. Usually, the pressure was calibrated twice, i.e., before and after each transport measurement. Then the average pressure was taken in the figures.

The dc electrical transport measurements were carried out in a physical property measurement system (PPMS-9 T, Quantum Design). For $\rho(T)$ measurements, the electrodes from the same side of the rectangular sample were set as current source or voltage output. To get precise measurement results, we used a constant temperature sweeping rate of 0.5 K/min across the superconducting transitions. For temperatures above T_c, the temperature sweeping rate is set as 1 K/min for all the measurements under different pressures, which enables the accurate analysis of the normal-state transport behavior without the contamination from inconsistent measurement conditions. For Hall measurements, two pairs of diagonal electrodes were individually set as the current source and the Hall voltage output. Two different measurement strategies, namely, field sweeping and temperature sweeping methods, were adopted, and the measurement results are consistent. To cancel the electrode asymmetric factor, Hall resistivity is calculated via $\rho_{xy} = [\rho_{xy}(\mu_0 H > 0) - \rho_{xy}(\mu_0 H < 0)]/2$. A low-field high-pressure magnetization experiment was performed using a vibrating sample magnetometer integrated in PPMS on the basis of a commercial Be-Cu piston-cylinder pressure cell. Daphne 7373 was also used as the pressure transmitting medium. A superconducting Pb sample was used as a pressure gauge by measuring its pressure-dependent T_c.

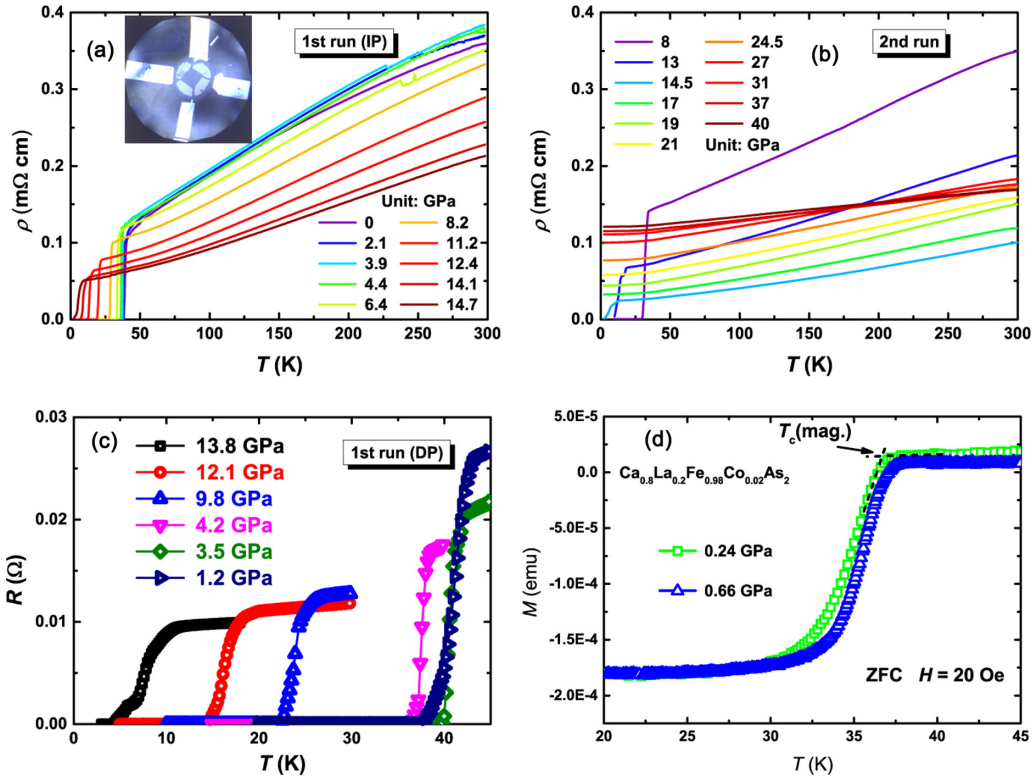

FIG. 2. (a, b) Temperature dependence of resistivity under different pressures during the pressure increasing (IP) process. Inset: Photograph of the sample and the electrical contacts inside the pressure chamber. (c) Temperature dependence of resistance under different pressures in the pressure releasing (DP) process. Superconductivity is found to be reversibly recovered. (d) Temperature dependence of magnetization of $Ca_{0.8}La_{0.2}Fe_{0.98}Co_{0.02}As_2$ under different pressures. The measurements were performed via a zero-field-cooling (ZFC) process under a magnetic field of $H = 20$ Oe.

III. RESULTS

As a small amount of Co doping can greatly improve the superconducting properties of the 112 system and results in a homogenous bulk superconductivity [24,26], sample $Ca_{1-x}La_xFe_{1-y}Co_yAs_2$ ($x = 0.2$, $y = 0.02$) was selected as the candidate for the high-pressure experiments. Figure 2 presents the main high-pressure experiment results. The sample shows a sharp superconducting transition around 37.5 K at ambient pressure. In the normal state, a downward curvature is evident in the $\rho(T)$ curve, which resembles those of Co-free 112-type crystals [25], $NdFeAsO_{1-x}F_x$ [10], and overdoped $Ba_{1-x}K_xFe_2As_2$ [28]. Upon applying pressure, the superconducting transition T_c shows somewhat subtle enhancement, which is further verified by the pressure-dependent magnetization measurements as shown in Fig. 2(d). This slight positive pressure dependence is analogous to what was seen in the optimally doped $Ba_{1-x}K_xFe_2As_2$ films [29]. At the low-pressure range of $P < 3.9$ GPa, the normal-state resistivity changes a little with varying pressures, and the downward curvature of normal-state $\rho(T)$ is gradually suppressed. At $P \sim 3.9$ GPa, T_c reaches the highest value while the resistivity above T_c grows linearly with temperature. As P increases over 3.9 GPa, T_c begins to decrease with pressure. Simultaneously, an upward curvature begins to be evident in an intermediate temperature range from T_c to about 150 K. At $P = 17$ GPa, superconductivity is totally suppressed. Upon releasing pressure, the superconductivity is found to be reversibly restored [see Fig. 2(c)]. From the later Hall measurements as shown below, applying high pressure in fact acts to increase electron doping. No reentrance of a second superconducting phase can be identified up to $P \sim 40$ GPa [see Fig. 2(b)]. Additionally, the AFM transition seen in NMR at the similar electron doping level does not seem to be reflected in the resistivity of our sample from the ambient pressure to the maximum pressure ($P \sim 40$ GPa). Compared with the previous results on $Ca_{1-x}La_xFeAs_2$ ($0.15 \leqslant x \leqslant 0.24$) [20] and $Ca_{1-x}La_xFe_{1-y}Co_yAs_2$ ($x = 0.27$) [22] (see Fig. 1), the absence of AFM order in our studied sample may suggest the different doping mechanisms between the Ca-site doping and the Fe-site doping.

In Fig. 3, we further analyzed the normal-state resistivity according to the power-law scaling, i.e., $\rho(T) = \rho_0 + AT^\alpha$, where α is the temperature exponent, ρ_0 is the residual resistivity, and the prefactor A is a parameter related not only to electron-electron interactions but also to other interactions like electron-phonon coupling via the effective mass m^*. For a FL, $\alpha = 2$ and A is determined by electron-electron scattering. As seen, at low temperatures, all $\rho(T)$ curves under different pressures nicely follow the power-law behaviors. For $P < 3.9$ GPa, the α values from the fitting are smaller than 1, indicative of substantial deviations from the FL behaviors. As P increases, the α value grows gradually. At $P = 3.9$ GPa, a linear T dependence of ρ is seen [inset in Fig. 3(a)]. It should be pointed out that strictly linear $\rho(T)$ has also been previously observed in other Fe-based systems like $BaFe_2As_{2-x}P_x$ [13,14] and $BaFe_{2-x}Ru_xAs_2$ [15], which has

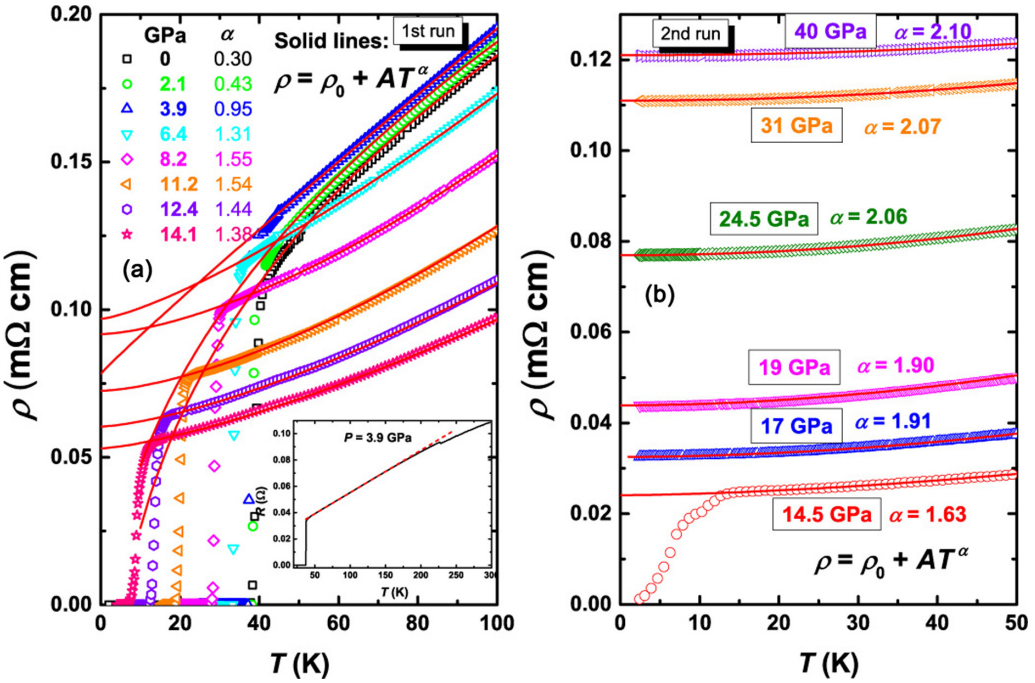

FIG. 3. (a, b) Power-law ($\rho(T) = \rho_0 + AT^{\alpha}$) fitting of the normal-state resistivity above T_c. The inset in (a) shows the linear $\rho(T)$ behavior within a wide temperature range at $P = 3.9$ GPa. The red dashed line is a guide to the eyes and the jump at ~230 K is the measurement noise.

attracted great attention due to the possible existence of a magnetic QCP. To date, whether there is a correlation between the linear $\rho(T)$ and a QCP is still an open question [4,12,30]. In this 112 system, the T-linear resistivity is likely a crossover from $\alpha < 1$ to $\alpha > 1$. As P increases further, the α value increases continuously until it saturates to $\alpha \sim 2$ at $P =$ 17 GPa, precisely where the superconductivity disappears. For $P \geqslant 17$ GPa, the low-temperature resistivity nicely obeys the T^2 rule, consistent with a FL ground state.

The T dependence of exponent α is summarized in Fig. 4. As seen, α keeps increasing from a value smaller than 1 at very low pressures to 2 for $P \geqslant 17$ GPa. Here, we emphasize

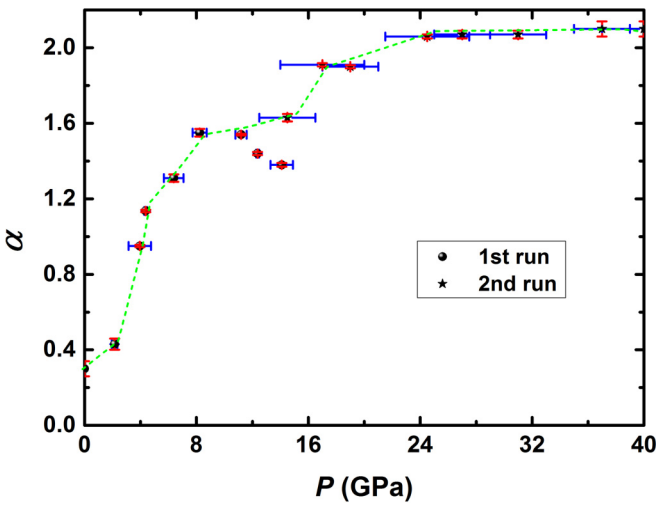

FIG. 4. Pressure dependence of the exponent α based on the power-law fitting in Fig. 3. See the discussion on the large error bars of the second run in Ref. [27].

several distinct features by comparing the pressure effect of the present 112 system with the chemical doping effect in $BaFe_2As_{2-x}P_x$ or in $BaFe_{2-x}Ru_xAs_2$. In the latter two cases [13–15], AFM transition coexists with superconductivity in the underdoped region, and is gradually suppressed with increasing doping. At the optimally doped level, α is equal to 1. At the same time, AFM disappears and superconducting T_c reaches its maximum. Below or above the optimal doping level, α is greater than 1. As a result, a V-shaped $\alpha(x)$ relation is observed. Here, α increases monotonously with P, and no adjacency to a *static* AFM phase transition can be identified in the resistivity. Therefore no indication of the possible QCP can be identified in the present system. The residual resistivity ρ_0 and the prefactor A obtained through FL fitting above 17 GPa are shown in Ref. [27] (Fig. S3). Broadly speaking, in the framework of a FL theory, the prefactor A is proportional to the charge-carrier effective mass m^*. The suppression of A with P suggests a reduced m^*, signifying gradual loss of electron correlations after superconductivity is suppressed.

To proceed, we measured the Hall resistivity under different pressures. As seen from Fig. 5, the calculated Hall coefficients (R_H) from the field sweeping method and the temperature sweeping method show comparable values and consistent T dependencies. At ambient pressure, the $R_H(T)$ curve exhibits an obvious extremum at a characteristic temperature $T_H \sim$ 180 K. Considering a single unit cell, the nominal doping carrier number is 0.22 per Fe atom based on the chemical stoichiometry of the sample. Then the nominal carrier density n_e can be estimated to be $n_e = 0.22/V$, where V is the volume of a single unit cell. Such a method leads to $|R_H| = 1/n_e \simeq 4.5 \times 10^{-9}$ m^3/C. As can be seen from Fig. 5, this $|R_H|$ value is almost one order of magnitude lower than the experimental values. As pressure increases, while the characteristic T_H of

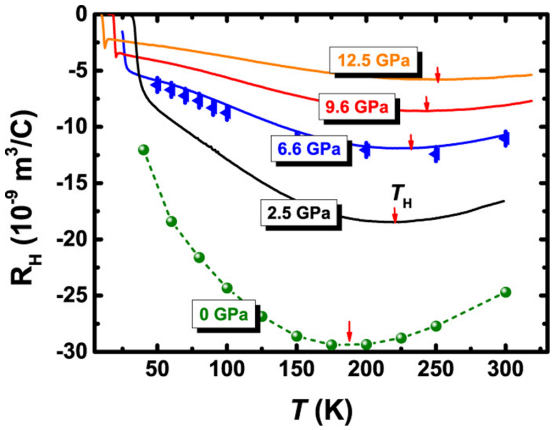

FIG. 5. Temperature dependence of Hall coefficient R_H under different pressures. The solid lines represent the measurements by T-sweeping method. The symbols stand for measurements by field-sweeping method. Both methods get consistent results. The temperature location of the extremum in the $R_H(T)$ curve is labeled by T_H.

the R_H extremum tends to move toward higher temperatures, the R_H extremum seems to be wiped out. At the same time, the absolute values of R_H decrease rapidly with increasing P, indicating a notable electron doping by pressure.

The above experimental results are summarized in the pressure-dependent phase diagram in Fig. 6. In this $T-P$ diagram, a superconducting dome is revealed with the pronounced normal-state NFL behaviors and monotonous $\alpha(P)$. Superconductivity disappears exactly when the NFL ground state is taken over by the FL. The simultaneous loss of T_c and the NFL behaviors imply the same governing mechanism for both phenomena.

We further investigate the evolution of the upper critical field H_{c2} ($H \parallel c$ axis) under pressure. In Fig. 7, the superconducting transitions under different magnetic fields and the temperature dependence of H_{c2} for different pressures are shown. In Fe-based superconductors, it is generally perceived that the single-band Werthamer-Helfand-Hohenberg (WHH)

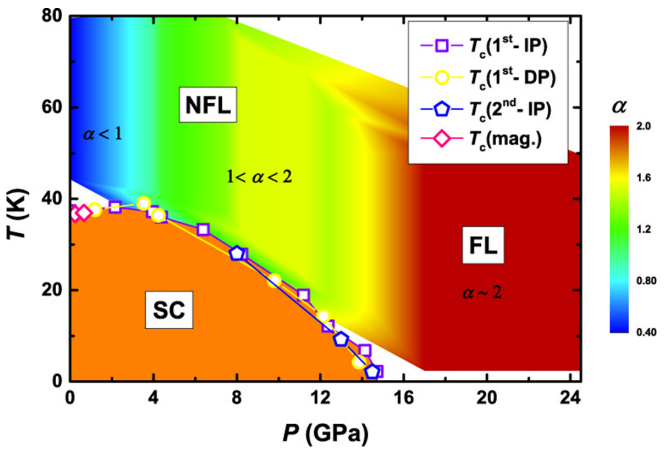

FIG. 6. Pressure phase diagram. The evolution of the exponent α (indicated by color mapping) from the power-law fitting and the superconducting transition temperature T_c vs pressure.

theory involved with spin-paramagnetic effect via the Maki parameter α_M and the spin-orbit interaction constant λ can overall fit the experimental H_{c2} for $H \parallel ab$, while for H_{c2} along the c axis the two-band model has to be considered [31–33]. In the absence of both spin-paramagnetic effect ($\alpha_M = 0$) and spin-orbit interaction ($\lambda = 0$), the WHH formula can be simplified as [34]

$$\ln\frac{1}{t} = \sum_{\nu=-\infty}^{\infty}\left\{\frac{1}{|2\nu+1|} - [|2\nu+1| + \frac{\overline{h}}{t}]\right\}, \qquad (1)$$

where $t = T/T_c$ and $\overline{h} = (4/\pi^2)[\frac{H_{c2}(T)}{\frac{dH_{c2}}{dt}}|_{T_c}]$. At $P = 14.1$ GPa, as seen, a WHH fit with $\alpha = 0, \lambda = 0$ can reproduce the experimental data very well. However, at lower pressures, WHH fitting curves slightly fall below the experimental H_{c2} data. Alternatively, a two-band description of $H_{c2}(T)$ as in MgB_2 should be applied. The two-band model is expressed as [35]

$$a_0[\ln t + U(h)][\ln t + U(\eta h)] + a_2[\ln t + U(\eta h)] + a_1[\ln t + U(h)] = 0. \qquad (2)$$

Here, a_0, a_1, and a_2 are determined by λ matrix $\begin{pmatrix}\lambda_{11} & \lambda_{12}\\ \lambda_{21} & \lambda_{22}\end{pmatrix}$, where λ_{11}, λ_{22} and λ_{12}, λ_{21} are intraband and interband coupling constants. $U(x) = \psi(1/2+x) - \psi(1/2)$, where $\psi(x)$ is the digamma function. $h = H_{c2}D_1/2\phi_0 T$ and the band diffusivity ratio $\eta = D_2/D_1$, where ϕ_0 is the flux quantum and D_1 and D_2 are diffusivities of different bands. We first assume an intraband-dominant coupling with $\lambda = \begin{pmatrix}0.5 & 0.25\\ 0.25 & 0.5\end{pmatrix}$, i.e., $w = \lambda_{11}\lambda_{22} - \lambda_{12}\lambda_{21} > 0$, which is often used for Fe-based superconductors. Then, we only tune D_1 and η to fit the experimental data. As seen from Figs. 7(d)–7(f), the modeling of $H_{c2}(T)$ based on the two-band model is clearly better in comparison with the WHH fits for pressure $P = 9.8$ and 12.1 GPa. We further adopt an interband-dominant coupling with $\lambda = \begin{pmatrix}0.25 & 0.5\\ 0.5 & 0.25\end{pmatrix}$, i.e., $w = \lambda_{11}\lambda_{22} - \lambda_{12}\lambda_{21} < 0$, to fit the experimental $H_{c2}(T)$. As can be seen, the fittings are also reasonable, and the values of D_1 and η versus P develop the same trend as the intraband-dominant case. For $P = 14.1$ GPa, the obtained η values for both cases are around 1. $\eta = 1$ indicates equal band diffusivities for the two bands, which in fact reduces to the single-band WHH model in the dirty limit. The WHH and two-band fitting parameters are listed in Table I for completeness. Note that our analysis is rather independent of criteria used in determining H_{c2}. Here we define H_{c2} as the peak in $\frac{\partial\rho}{\partial T}(T)$ curves under individual fields. We also use the criterion of 90% of the normal state ρ_n (see Ref. [27]) and get the same results.

IV. DISCUSSIONS AND CONCLUSION

A strong temperature dependence of R_H, in particular the extremum around 180 K at ambient pressure, is striking, which was seen in some other Fe-based superconductors, such as the 122 pnictides as well as LiFeAs and LiFeP [8,11]. Many theoretical works *all* emphasize the anisotropic interband scattering between electronlike and holelike Fermi surfaces as the possible origin for this Hall coefficient extremum [6,36,37]. The most likely source for this anisotropic scattering is thought

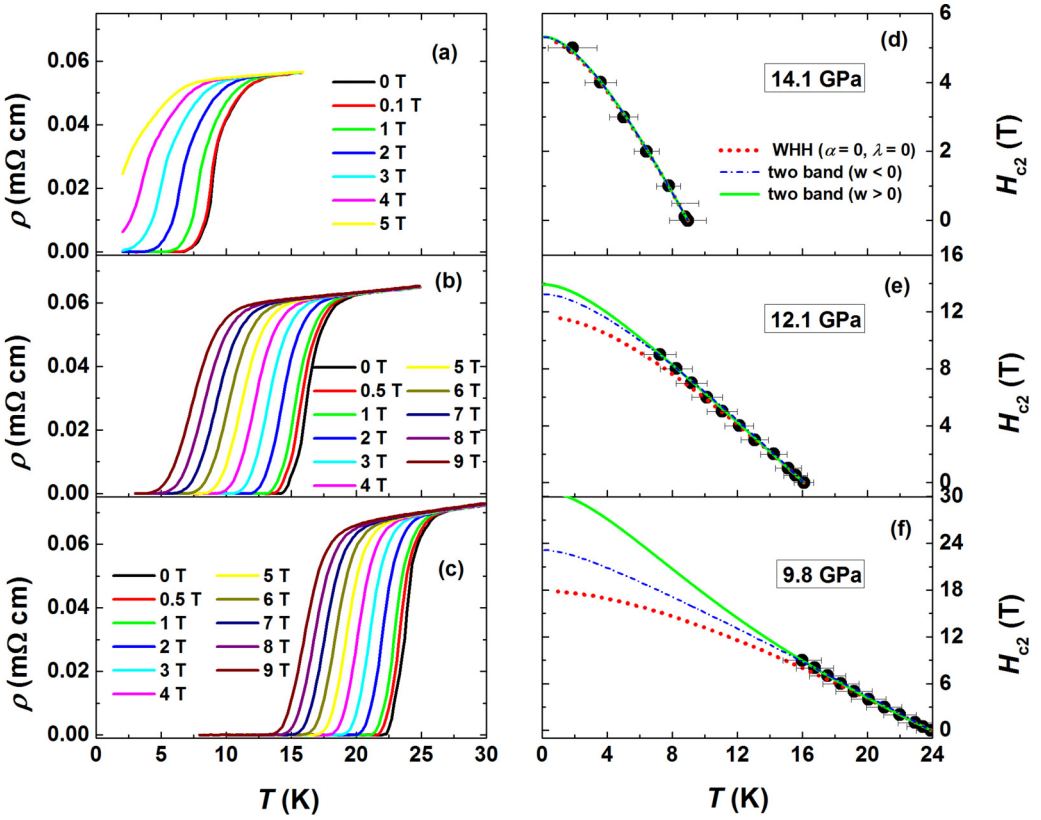

FIG. 7. (a–c) Temperature dependence of superconducting transitions under different magnetic fields applied along the c axis for pressure $P = 14.1$, 12.1, and 9.8 GPa, respectively. (d–f) Temperature dependence of the upper critical field H_{c2} which is extracted by the peak criterion, i.e., the peak position on $\frac{\partial \rho}{\partial T}(T)$ curves. The green solid lines and the blue dash-dotted lines are two-band fittings for $H_{c2}(T)$ with $w > 0$ and $w < 0$, respectively. The red dotted lines are WHH fits without considering spin-paramagnetic effect ($\alpha = 0$) and spin-orbit interaction ($\lambda = 0$). The error bars are determined by half of the difference of $H_{c2}(T)$ between the peak criterion and the 90% criterion, which must be larger than the maximum fluctuation of actual $H_{c2}(T)$. The 90% criterion defines H_{c2} by 90% of the normal-state resistivity just above T_c.

to come from the SFs, which induce a mixing of electron and hole currents such that the renormalized current in each band can even possess an opposite direction (negative transport time) with respect to the bare band velocity. In this picture, the $|R_H|$ extremum tends to be high for higher scattering anisotropy between electron (e) and hole (h) bands. The suppression of the Hall extremum under pressure seems to imply the decrease of anisotropic scattering and hence the weakening of SFs with pressure. Indeed, the suppression of the $|R_H|$ extremum with increasing P is also compatible with the T_c decrease, which favors the widely perceived pairing picture for iron pnictides, namely, SF mediated pairing. This in turn supports that the NFL in the normal state is also induced by SFs.

As we found, the downward curvature ($\alpha < 1$) in $\rho(T)$ curves at low pressures was also reported in the high-T phase of overdoped $Ba_{1-x}K_xFe_2As_2$ superconductors [8,28,38], where a crossover from high-T incoherent state ($\alpha < 1$) to low-T coherent state ($\alpha > 1$) was claimed to be seen. In our system, the suppression of the incoherent state with pressure up to optimal pressure (3.9 GPa) seems to explain the initial increase of T_c under pressure.

Finally, the pressure dependence of H_{c2} is also in favor of the above SF picture. At low pressures, SFs are strong, which favors the strong anisotropic superconducting gap or two gaps in the electronic spectrum. Our previous high-field experiments have given strong evidence for the two-band effects for the same sample at ambient pressure [39]. As

TABLE I. Parameters obtained from the WHH and two-band fittings. H_{c2}^{WHH} is from WHH fitting, and H_{c2}^{two} is from two-band fitting. $w = \lambda_{11}\lambda_{22} - \lambda_{12}\lambda_{21}$.

P (GPa)	T_c(0 T) (K)	$-dH_{c2}/dT\|_{T_c}$ (T/K)	H_{c2}^{WHH}(0 K) (T)	$w > 0$ H_{c2}^{two}(0 K) (T)	$w > 0$ D_1	$w > 0$ $\eta\ (=D_2/D_1)$	$w < 0$ H_{c2}^{two}(0 K) (T)	$w < 0$ D_1	$w < 0$ $\eta\ (=D_2/D_1)$
14.1	8.95	0.85	5.24	5.31	1.28	1	5.31	1.35	0.9
12.1	16.08	1.05	11.81	13.92	1.5	0.4	13.25	1.45	0.37
9.8	23.89	1.08	17.79	30.61	1.8	0.18	23.18	1.62	0.18
0 [39]	38.8	2.26	61	88.34	2.4	0.13			

pressure increases, SFs become effectively reduced and the band diffusivity ratio $\eta = D_2/D_1$ increases toward 1. $\eta = 1$ suggests more similar intraband scattering in the electron (e) and the hole (h) Fermi sheets, which ultimately leads to the thermodynamically isotropic gap (one gap). Overall, the above pressure dependence of T_c, R_H, and H_{c2}, as well as the NFL to FL crossover, all seem to support the picture that the SFs are suppressed by pressure and the superconductivity in this system is indeed mediated by SFs.

In summary, we have investigated the superconductivity and the normal-state transport behaviors in a 112-type superconductor $Ca_{1-x}La_xFe_{1-y}Co_yAs_2$ ($x = 0.2$, $y = 0.02$) in a broad pressure range up to 40 GPa. In the $T - P$ phase diagram, it is found, the normal state of the whole superconducting region is accompanied with the non-Fermi-liquid behaviors which turn into Fermi-liquid behaviors when superconductivity is totally suppressed. Exceptionally, no evidence of static AFM order is observed by transport measurement accompanying the non-Fermi-liquid region. Detailed study on the pressure evolution of the notable R_H extremum and the two-band nature of H_{c2} suggests non-negligible influence from the anisotropic scattering between electron and hole bands which is presumably caused by the spin fluctuations.

ACKNOWLEDGMENTS

We appreciate fruitful discussions with M. Breitkreiz and C. Timm, and careful proofreading by A. Bangura. This work was supported by the National Natural Science Foundation of China (Grants No. U1432135, No. 11704047, No. 11611140101, and No. 11674054). X.X. acknowledges financial support from the National Key Basic Research Program of China (Grant No. 2014CB648400) and from National Natural Science Foundation of China (Grants No. 11474080 and No. U1732162). B.Q. was supported partly by the Natural Science Foundation of Jiangsu Province (Grant No. BK20150831), Natural Science Foundation of Jiangsu Educational Department (Grant No. 15KJA430001), and six-talent peak of Jiangsu Province (Grant No. 2012-XCL-036).

W.Z. and F.K. contributed equally to this paper.

[1] Y. Ando, S. Komiya, K. Segawa, S. Ono, and Y. Kurita, Electronic Phase Diagram of High-T_c Cuprate Superconductors from a Mapping of the In-Plane Resistivity Curvature, Phys. Rev. Lett. **93**, 267001 (2004).

[2] Y. Dagan, M. M. Qazilbash, C. P. Hill, V. N. Kulkarni, and R. L. Greene, Evidence for a Quantum Phase Transition in $Pr_{2-x}Ce_xCuO_{4-\delta}$ from Transport Measurements, Phys. Rev. Lett. **92**, 167001 (2004).

[3] R. Daou, N. Doiron-Leyraud, D. LeBoeuf, S. Y. Li, F. Laliberté, O. Cyr-Choinière, Y. J. Jo, L. Balicas, J.-Q. Yan, J.-S. Zhou, J. B. Goodenough, and L. Taillefer, Linear temperature dependence of resistivity and change in the Fermi surface at the pseudogap critical point of a high-T_c superconductor, Nat. Phys. **5**, 31 (2009).

[4] J. G. Analytis, H-H. Kuo, R. D. McDonald, M. Wartenbe, P. M. C. Rourke, N. E. Hussey, and I. R. Fisher, Transport near a quantum critical point in $BaFe_2(As_{1-x}P_x)_2$, Nat. Phys. **10**, 194 (2014).

[5] Y. M. Dai, B. Xu, B. Shen, H. Xiao, H. H. Wen, X. G. Qiu, C. C. Homes, and R. P. S. M. Lobo, Hidden T-Linear Scattering Rate in $Ba_{0.6}K_{0.4}Fe_2As_2$ Revealed by Optical Spectroscopy, Phys. Rev. Lett. **111**, 117001 (2013).

[6] L. Fanfarillo, E. Cappelluti, C. Castellani, and L. Benfatto, Unconventional Hall Effect in Pnictides from Interband Interactions, Phys. Rev. Lett. **109**, 096402 (2012).

[7] X. Ding, Y. Pan, H. Yang, and H.-H. Wen, Strong and nonmonotonic temperature dependence of Hall coefficient in superconducting $K_xFe_{2-y}Se_2$ single crystals, Phys. Rev. B **89**, 224515 (2014).

[8] K. Ohgushi and Y. Kiuchi, Doping dependence of Hall coefficient and evolution of coherent electronic state in the normal state of the Fe-based superconductor $Ba_{1-x}K_xFe_2As_2$, Phys. Rev. B **85**, 064522 (2012).

[9] J. C. Zhuang, W. K. Yeoh, X. Y. Cui, J. H. Kim, D. Q. Shi, Z. X. Shi, S. P. Ringer, X. L. Wang, and S. X. Dou, Enhancement of transition temperature in $Fe_xSe_{0.5}Te_{0.5}$ film via iron vacancies, Appl. Phys. Lett. **104**, 262601 (2014).

[10] P. Cheng, H. Yang, Y. Jia, L. Fang, X. Zhu, G. Mu, and H.-H. Wen, Hall effect and magnetoresistance in single crystals of $NdFeAsO_{1-x}F_x$ ($x = 0$ and 0.18), Phys. Rev. B **78**, 134508 (2008).

[11] S. Kasahara, K. Hashimoto, H. Ikeda, T. Terashima, Y. Matsuda, and T. Shibauchi, Contrasts in electron correlations and inelastic scattering between LiFeP and LiFeAs revealed by charge transport, Phys. Rev. B **85**, 060503(R) (2012).

[12] Y. M. Dai, H. Miao, L. Y. Xing, X. C. Wang, P. S. Wang, H. Xiao, T. Qian, P. Richard, X. G. Qiu, W. Yu, C. Q. Jin, Z. Wang, P. D. Johnson, C. C. Homes, and H. Ding, Spin-Fluctuation-Induced Non-Fermi-Liquid Behavior with Suppressed Superconductivity in $LiFe_{1-x}Co_xAs$, Phys. Rev. X **5**, 031035 (2015).

[13] S. Jiang, H. Xing, G. Xuan, C. Wang, Z. Ren, C. Feng, J. Dai, Z. Xu, and G. Cao, Superconductivity up to 30 K in the vicinity of the quantum critical point in $BaFe_2(As_{1-x}P_x)_2$, J. Phys.: Condens. Matter **21**, 382203 (2009).

[14] S. Kasahara, T. Shibauchi, K. Hashimoto, K. Ikada, S. Tonegawa, R. Okazaki, H. Shishido, H. Ikeda, H. Takeya, K. Hirata, T. Terashima, and Y. Matsuda, Evolution from non-Fermi- to Fermi-liquid transport via isovalent doping in $BaFe_2(As_{1-x}P_x)_2$ superconductors, Phys. Rev. B **81**, 184519 (2010).

[15] M. J. Eom, S. W. Na, C. Hoch, R. K. Kremer, and J. S. Kim, Evolution of transport properties of $BaFe_{2-x}Ru_xAs_2$ in a wide range of isovalent Ru substitution, Phys. Rev. B **85**, 024536 (2012).

[16] T. Hu, Y. P. Singha, L. Shub, M. Janoschekb, M. Dzeroa, M. B. Mapleb, and C. C. Almasan, Non-Fermi liquid regimes with and without quantum criticality in $Ce_{1-x}Yb - xCoIn_5$, Proc. Natl. Acad. Sci. USA **110**, 7160 (2013).

[17] N. Katayama, K. Kudo, S. Onari, T. Mizukami, K. Sugawara, Y. Sugiyama, Y. Kitahama, K. Iba, K. Fujimura, N. Nishimoto, M. Nohara, and H. Sawa, Superconductivity in $Ca_{1-x}La_xFeAs_2$: A novel 112-type iron pnictide with arsenic zigzag bonds, J. Phys. Soc. Jpn. **82**, 123702 (2013).

[18] H. Yakita, H. Ogino, T. Okada, A. Yamamoto, K. Kishio, T. Tohei, Y. Ikuhara, Y. Gotoh, H. Fujihisa, K. Kataoka, H. Eisaki,

and J. Shimoyama, A new layered iron arsenide superconductor: (Ca, Pr)$FeAs_2$, J. Am. Chem. Soc. **136**, 846 (2014).

[19] Y. Huang, X.-L. Yu, D.-Y. Liu, and L.-J. Zou, Magnetism and electronic structures of novel layered $CaFeAs_2$ and $Ca_{0.75}(Pr/La)_{0.25}FeAs_2$, J. Appl. Phys. **117**, 17E113 (2015).

[20] S. Kawasaki, T. Mabuchi, S. Maeda, T. Adachi, T. Mizukami, K. Kudo, M. Nohara, and G.-Q. Zheng, Doping-enhanced antiferromagnetism in $Ca_{1-x}La_xFeAs_2$, Phys. Rev. B **92**, 180508(R) (2015).

[21] S. Jiang, C. Liu, H. Cao, T. Birol, J. M. Allred, W. Tian, L. Liu, K. Cho, M. J. Krogstad, J. Ma, K. M. Taddei, M. A. Tanatar, M. Hoesch, R. Prozorov, S. Rosenkranz, Y. J. Uemura, G. Kotliar, and N. Ni, Structural and magnetic phase transitions in $Ca_{0.73}La_{0.27}FeAs_2$ with electron-overdoped FeAs layers, Phys. Rev. B **93**, 054522 (2016).

[22] S. Jiang, L. Liu, M. Schutt, A. M. Hallas, B. Shen, W. Tian, E. Emmanouilidou, A. Shi, G. M. Luke, Y. J. Uemura, R. M. Fernandes, and N. Ni, Effect of interlayer coupling on the coexistence of antiferromagnetism and superconductivity in Fe pnictide superconductors: A study of $Ca_{0.74(1)}La_{0.261}(Fe_{1-x}Co_x)As_2$ single crystals, Phys. Rev. B **93**, 174513 (2016).

[23] Y. Zhou, S. Jiang, Q. Wu, V. A. Sidorov, J. Guo, W. Yi, S. Zhang, Z. Wang, H. Wang, S. Cai, K. Yang, S. Jiang, A. Li, N. Ni, G. Zhang, L. Sun, and Z. Zhao, Observation of a bi-critical point between antiferromagnetic and superconducting phases in pressurized single crystal $Ca_{0.73}La_{0.27}FeAs_2$, Sci. Bull. **62**, 857 (2017).

[24] X. Xing, W. Zhou, N. Zhou, F. Yuan, Y. Pan, H. Zhao, X. Xu, and Z. Shi, Anisotropic Ginzburg-Landau scaling of H_{c2} and transport properties of 112-type $Ca_{0.8}La_{0.2}Fe_{0.98}Co_{0.02}As_2$ single crystal, Supercond. Sci. Technol. **29**, 055005 (2016).

[25] W. Zhou, J. C. Zhuang, F. Yuan, X. Li, X. Z. Xing, Y. Sun, and Z. Shi, Anisotropic superconductivity of $Ca_{1-x}La_xFeAs_2$ ($x \sim 0.18$) single crystal, Appl. Phys. Express **7**, 063102 (2014).

[26] X. Xing, W. Zhou, B. Xu, N. Li, Y. Sun, Y. Zhang, and Z. Shi, Co-co-doping effect on superconducting properties of 112-type $Ca_{0.8}La_{0.2}FeAs_2$ single crystals, J. Phys. Soc. Jpn. **84**, 075001 (2015).

[27] See Supplemental Material at http://link.aps.org/supplemental/10.1103/PhysRevB.96.184503 for discussions of the pressure homogeneity, the power-law analysis of normal-state resistivity, and the behavior of upper critical field H_{c2}.

[28] B. Shen, H. Yang, Z.-S. Wang, F. Han, B. Zeng, L. Shan, C. Ren, and H.-H. Wen, Transport properties and asymmetric scattering in $Ba_{1-x}K_xFe_2As_2$ single crystals, Phys. Rev. B **84**, 184512 (2011).

[29] E. Park, N. H. Lee, W. N. Kang, and T. Park, Pressure effects on the superconducting thin film $Ba_{1-x}K_xFe_2As_2$, Appl. Phys. Lett. **101**, 042601 (2012).

[30] D. Hu, X. Lu, W. Zhang, H. Luo, S. Li, P. Wang, G. Chen, F. Han, S. R. Banjara, A. Sapkota, A. Kreyssig, A. I. Goldman, Z. Yamani, C. Niedermayer, M. Skoulatos, R. Georgii, T. Keller, P. Wang, W. Yu, and P. Dai, Structural and Magnetic Phase Transitions Near Optimal Superconductivity in $BaFe_2(As_{1-x}P_x)_2$, Phys. Rev. Lett. **114**, 157002 (2015).

[31] A. Gurevich, Iron-based superconductors at high magnetic fields, Rep. Prog. Phys. **74**, 124501 (2011).

[32] D. A. Zocco, K. Grube, F. Eilers, T. Wolf, and H. v. Löhneysen, Pauli-Limited Multiband Superconductivity in KFe_2As_2, Phys. Rev. Lett. **111**, 057007 (2013).

[33] Z. Wang, T. Xie, E. Kampert, T. Förster, X. Lu, R. Zhang, D. Gong, S. Li, T. Herrmannsdörfer, J. Wosnitza, and H. Luo, Electron doping dependence of the anisotropic superconductivity in $BaFe_{2-x}Ni_xAs_2$, Phys. Rev. B **92**, 174509 (2015).

[34] N. R. Werthamer, E. Helfand, and P. C. Hohenberg, Temperature and purity dependence of the superconducting critical field, H_{c2}. III. Electron spin and spin-orbit effects, Phys. Rev. **147**, 295 (1966).

[35] A. Gurevich, Enhancement of the upper critical field by nonmagnetic impurities in dirty two-gap superconductors, Phys. Rev. B **67**, 184515 (2003).

[36] M. Breitkreiz, P. M. R. Brydon, and C. Timm, Transport anomalies due to anisotropic interband scattering, Phys. Rev. B **88**, 085103 (2013).

[37] M. Breitkreiz, P. M. R. Brydon, and C. Timm, Transport in multiband systems with hot spots on the Fermi surface: Forward-scattering corrections, Phys. Rev. B **89**, 245106 (2014).

[38] Y. Liu and T. A. Lograsso, Crossover in the magnetic response of single-crystalline $Ba_{1-x}K_xFe_2As_2$ and Lifshitz critical point evidenced by Hall effect, Phys. Rev. B **90**, 224508 (2014).

[39] X. Xing, W. Zhou, J. Wang, Z. Zhu, Y. Zhang, N. Zhou, B. Qian, X. Xu, and Z. Shi, Two-band and Pauli-limiting effects on the upper critical field of 112-type iron pnictide superconductors, Sci. Rep. **7**, 45943 (2017).